Sensitivity analysis of directivity effects on PSHA

E. Chioccarelli and I. Iervolino

Dipartimento di Ingegneria Strutturale, Università Federico II, Napoli, Italy

ABSTRACT Careful characterization of seismic hazard is especially important in structural engineering if critical facilities (e.g., strategic buildings, chemical deposits, energy production plants, etc.) are the object of analysis. Moreover, if the construction site is close to active faults, particular attention is required. In fact, in this condition, the fault's dynamics affect ground motion differently from site to site, resulting in systematic spatial variability, and, generally, in higher seismic demand, with respect to the far-source case. The most important of the near-source (NS) effects is known as *forward rupture directivity*, and can be identified by a large full-cycle pulse at the beginning of the velocity records, and containing the most of carried energy. Recent research demonstrates that, from the structural engineering point of view, hazard assessment should account for NS effects (i.e., pulse-like ground motions), but ordinary probabilistic seismic hazard analysis (PSHA) is not able to do it appropriately. On the other hand, semi-empirical models calibrated for introducing NS effects in classical PSHA are now available, and some preliminary attempts of numerical implementation of NS-PSHA exist. In the presented study, numerical applications of strike-slip (SS) fault scenarios are provided and, for a fixed return period, uniform hazard spectra are computed in order to quantify hazard increments (*HIs*) due to NS-PSHA with respect to ordinary-PSHA. It is shown that: i) depending on source-site geometry, these may be significant (more than a 100% increment); ii) different spectral periods are affected by significantly different values of *HIs*, which have their shape controlled only by the magnitude of generated earthquakes; iii) it is possible to identify a zone beyond which directivity effects are expected to become negligible, at least with a first-order approximation, independently of the characteristics of the considered SS fault.

Key words: hazard increments, pulse-like records, near-fault, fault scenario.

1. Introduction

In near-source (NS) conditions, ground motions and seismic structural response, may show spatial variability systematically different from what shown in far-source condition. This is mainly because of rupture's *forward directivity*, which may most likely affect near-fault sites in particular geometrical configurations with respect to the rupture. The resulting phenomenon, of largest engineering interest, is a large full-cycle pulse at the beginning of velocity record

containing most of its energy, and mainly observed in fault-normal (FN) component (Somerville *et al.*, 1997)[1].

A discussion of directivity effects was given with respect to the recent L'Aquila 2009 (central Italy) earthquake (moment magnitude equal to 6.3), and a detailed analysis can be found in Chioccarelli and Iervolino (2010). In this same study, analyzing a large American data set [next generation attenuation (NGA) database, http://peer.berkeley.edu/nga/ (last access June 2013)], three main features of engineering interest characterizing pulse-like records, if compared to those non-pulse-like (hereafter referred to as *ordinary*), were found: 1) pulse-like signals are characterized by FN components generally *stronger* than fault parallel (FP) (non-pulse-like ground motions have equivalent median FN and FP components); 2) FN pulse-like signals are characterized by a non-standard spectral shape with an increment of spectral ordinates in a range around the pulse period (T_p); 3) the C_R factor, defined as the ratio between inelastic spectral displacements [of a single degree of freedom (SDoF) system with given strength reduction factor, R_S] to the corresponding elastic spectral displacement, can be, for FN pulse-like records, 20% ÷ 70% larger than that of ordinary motions, depending on the non-linearity level (see also Iervolino *et al.*, 2012). Such increments are displayed in a range of periods between about 30% and 50% of pulse period. This is especially relevant for earthquake resistant structural design and assessment. An analysis of inelastic displacement demand associated to forward-directivity ground-motions is also provided in Ruiz-Garcìa (2011).

In Fig. 1a, the average of the FN elastic spectra, normalized to peak ground acceleration (*PGA*) is given for pulse-like records considered herein, with T_p between 1 and 2 s (Average Pulse), and for ordinary ground motions (Average Non Pulse), both taken from NGA. In Fig. 1b, referring to the same database, C_R for an $R_S = 4$ is given for pulse-like and non-pulse-like records (Pulse - FN and Non Pulse - FN, respectively). The figures allow the appreciation of the systematic differences summarized above, especially points 2) and 3), among the considered classes[2]. Moreover, C_R for the FP components of the pulse-like FN records (which not necessarily are pulse-like, even if indicated as *Pulse - FP*), is shown: it appears that FP records have a shape similar to FN in the low T/T_p range, yet with lower amplitudes.

Identification of design seismic actions is a fundamental step in the assessment of structural seismic risk and the most consolidated framework to deal with this issue is the probabilistic seismic hazard analysis (PSHA) (Cornell, 1968; McGuire, 2004): it allows to build hazard curves for selected ground motion intensity measures (IMs), starting from seismic source models and ground motion prediction equations (GMPEs). However, it has been formulated for ordinary conditions and needs adjustments for sites close to a seismic fault and, then, potentially subjected to pulse-like directivity effects. Therefore, because ordinary PSHA is adopted by most advanced seismic codes worldwide (e.g., CEN, 2003; C.S.LL.PP., 2008), such codes provide design actions with respect to which directivity may represent an unexpected demand. This seems especially important in the case of critical structures. On the other hand, NS-PSHA

---

[1] Generally, in seismology the term directivity is used to indicate the azimuthal variation of the radiated seismic energy due to the geometry of the rupture growth (Boatwright and Boore, 1982). In this study, the term directivity is referred to the physical phenomena producing pulse-like ground motions.

[2] A T_P can be assigned also to ordinary records (even if non-significant), rendering possible a representation as a function of T/T_P.
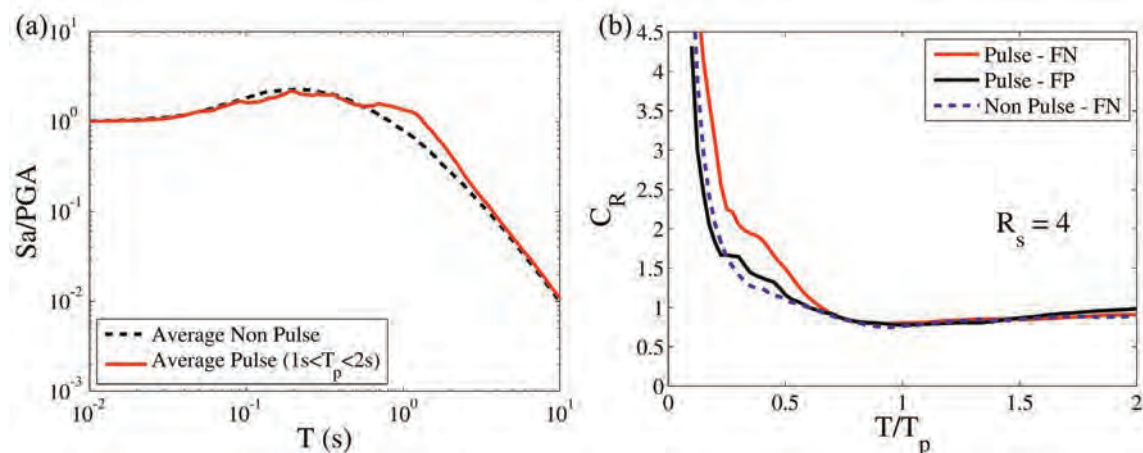
Fig. 1 - a) Elastic 5% damped spectra for FN pulse-like with 1 s < T_p < 2 s and ordinary records; b) empirical C_R for FN pulse-like records, for their FP components, and for ordinary records, at $R_S = 4$. Figure adapted from Iervolino *et al.* (2012).

requires an increased computational effort because, as shown in the following, additional random variables are involved with respect to the classical case.

The aim of this work is to provide quantification of directivity effects in hazard assessment if compared to ordinary analysis, together with some preliminary indications about the geographic area around a strike-slip (SS) fault in which significant directivity effects should be expected.

The paper is structured so that modified PSHA accounting for pulse-like issues is presented first, recalling all the necessary models already available in literature. Then, some illustrative applications are carried out[3]; results of ordinary and modified PSHA are compared referring to a fixed return period of seismic action. Selecting a specific site, analyses of the whole pseudo-acceleration uniform hazard spectra (UHS) are shown, discussing trends of hazard increments (*HIs*) of NS - with respect to ordinary - PSHA. Moreover, directivity effects in the area around the fault are analyzed showing that, with a significant reduction of computational effort, a quantitative estimation of *HIs* in each site can be provided. Although results refer to the presented applications, trends expected to be systematic can be identified.

2. Modified PSHA for near-source conditions

As mentioned, ordinary PSHA cannot account for spatial ground motion variability, which may affect NS sites. More specifically, the two main limits can be found in the GMPEs, and in the identification of relative site-source configuration. In fact, ordinary GMPEs are fitted on ground motion databases in which pulse-like records, if any, are usually scarce, and often rotated differently to FN and FP directions. Moreover, because each record is characterized by a different

---

[3] All of them refer to single fault scenarios because NS-PSHA requires the knowledge of size and location of the rupture, and cannot be directly applied using seismic source zones (e.g., Meletti *et al.*, 2008). However, if critical facilities are of concern, it is reasonable to imagine a deeper knowledge of seismic faults in the building area.

T_p, the influence of pulse-like spectral shape on such GMPEs is masked and/or spread over a broad range of periods (Shahi and Baker, 2011). On the other hand, not all NS sites are equally prone to be subjected to directivity effects (Somerville *et al.*, 1997; Iervolino and Cornell, 2008) and the simple source-to-site distance, used in ordinary PSHA, is not enough to identify where probability of pulse-like records is larger.

Recent attempts in solving these issues were aimed at retaining the general PSHA framework, introducing some directivity-related adjustments (e.g., Abrahamson, 2000; Tothong *et al.*, 2007; Iervolino and Cornell, 2008). All required probabilistic models are available nowadays, and preliminary applications may be found in Chioccarelli (2010) and Shahi and Baker (2011).

Herein, in order to describe the modified procedure, the standard approach to PSHA is first recalled. Assuming a homogenous Poisson model of earthquake occurrence, Eq. (1) is used for computing the mean annual frequency (MAF, or λ_{IM}^{PSHA}) of exceeding a ground motion intensity measure threshold, in the case a single seismic source is considered. Hereafter, the chosen IM is the elastic spectral acceleration (S_a) at a fixed period T, that is $S_a(T)$. M is the magnitude of the earthquake (hereafter moment magnitude) and R is the source-to-site distance, ν is the mean annual rate of earthquakes occurrence on the source within a magnitude range of interest, $f_{M,R}$ is the joint probability density function (PDF) of M and R. Finally $G_{Sa|M,R}$ is the complementary cumulative distribution function (CCDF) of S_a (usually lognormal, if obtained by a GMPE).

$$\lambda_{Sa}^{PSHA}(S_a) = \nu \cdot \iint_{m\ r} G_{Sa|M,R}(S_a|m,r) \cdot f_{M,R}(m,r) \cdot dm \cdot dr \qquad (1)$$

NS-PSHA considers the MAF $\left(\lambda_{Sa}^{NS-PSHA}\right)$ to be a linear combination of two hazard terms which account for the absence or the occurrence of the pulse, $\lambda_{Sa,NoPulse}$ and $\lambda_{Sa,Pulse}$ respectively, as reported in Eq. (2).

$$\lambda_{Sa}^{NS-PSHA}(s_a) = \lambda_{Sa,NoPulse}(s_a) + \lambda_{Sa,Pulse}(s_a). \qquad (2)$$

The two terms of Eq. (2) are implicitly weighted by the pulse occurrence probability, $P[Pulse|\underline{Z}]$, which is provided by Iervolino and Cornell (2008).[4] The latter, in fact, depends on the relative source-site configuration, which is identified by simple geometrical parameters represented by the $\underline{Z}$ vector of variables. Such variables are known once rupture, hypocentre, and site positions are known. In the case of SS rupture (Fig. 2a), $\underline{Z}$ is comprised of rupture-to-site distance (R), the distance from the epicenter to the site measured along the rupture direction (s), and angle between the fault strike and the path from epicenter to the site (θ). It should be noted that the probability model in Iervolino and Cornell (2008) is defined for R, s and θ varying in the intervals of (0 - 30 km), (0 - 40 km) and (0° - 90°), respectively. In the applications to follow, zero pulse probabilities are associated to values outside the covariates' intervals where model applies.

Two other issues, which are not faced in traditional hazard analysis, appear in NS-PSHA: i) pulse period prediction; ii) pulse amplitude prediction.

---

[4] A model describing irregular spatial distribution of seismic effects is also provided by Spudich and Chiou (2008).
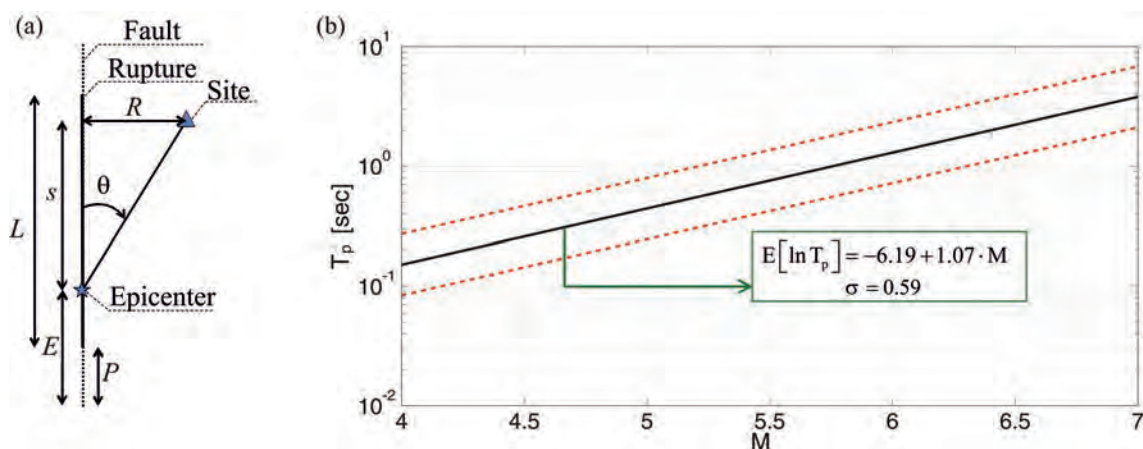
Fig. 2 - SS geometrical parameters in plan (a) and regression model for T_p (b).

The former (i) has been addressed by many authors referring to a lognormal random variable conditional on the event magnitude; i.e., $f_{T_p|M}(t_p|m)$, the parameters of which were retrieved on an empirical basis. The model considered herein is from Chioccarelli and Iervolino (2010) (Fig. 2b), but others are available; see Tang and Zhang (2010) for a review.

The latter issue (ii) should be accounted for fitting a new GMPE on pulse-like records generated by rupture directivity effects only. Alternatively, an easier procedure was proposed by Baker (2008) referring to the already available ordinary GMPE of Boore and Atkinson (2008) and modifying it in order to be representative of pulse-like spectra. Thus, the modification factor, operating on the mean value of logarithms of spectral pseudo-acceleration, is a function of T_p as shown in Eq. (3). It consists of adding a 'bump' of spectral ordinates around the pulse period. In the equation, $\ln(S_a(T))$ is the expected value of logarithms of spectral acceleration predicted by the original GMPE (G_{Sa} in the following), and $\ln(S_{a,mod}(T))$ is the value provided by modified GMPE ($G_{Sa,mod}$).

$$\ln\left(S_{a,\mathrm{mod}}\left(T\right)\right)=\ln\left(S_a\left(T\right)\right)+e^{-\left(\ln\left(T/T_p\right)\right)^2} . \tag{3}$$

Eqs. (4) and (5), expand Eq. (2) in the case of a single fault with SS style. In numerical applications of this rupture case (to follow), the geometrical parameters required by pulse occurrence probability model are transformed in the rupture length (L), the position of the rupture on the fault (P), and the epicenter location (E), as reported in Fig. 2a. A deterministic relationship between these parameters and $\{R,s,\theta\}$ vector exists. Thus, the $\underline{Z}$ vector can be replaced by a vector comprised of L, P and E. This allows to more easily simulate the uncertainty involved for hazard computations, that is, distributions can be conveniently assigned for $\{L,P,E\}$, then $\{R,s,\theta\}$ may be retrieved and pulse occurrence probability can be calculated:

$$\lambda_{Sa,NoPulse}\left(s_a\right)=v\cdot\iiiint\limits_{m\ l\ p\ e}P\left[NoPulse|l,p,e\right]\cdot G_{Sa|M,L,P}\left(s_a|m,l,p\right)\cdot$$
$$f_{P,E|L}\left(p,e|l\right)\cdot f_{L|M}\left(l|m\right)\cdot f_M\left(m\right)\cdot dm\cdot dl\cdot dp\cdot de \tag{4}$$

$$\lambda_{Sa,Pulse}(s_a) = \nu \cdot \int_{t_p} \int_m \int_l \int_p \int_e P[Pulse|l,p,e] \cdot G_{Sa,\text{mod}|T_p,M,L,P}(s_a|t_p,m,l,p)$$

$$f_{T_p|M}(t_p|m) \cdot f_{P,E|L}(p,e|l) \cdot f_{L|M}(l|m) \cdot f_M(m) \cdot dt_p \cdot dm \cdot dl \cdot dp \cdot de \,. \tag{5}$$

In Eqs. (4) and (5) statistical dependencies are explicitly indicated for all the distributions already introduced; indeed, $f_{P,E|L}(p,e|l)$ is the uniform distribution of P and E on the rupture length, $f_{L|M}(l|m)$ is the distribution of L on the event magnitude [provided by Wells and Coppersmith (1994)], $f_M(m)$ is the model of magnitude distribution.

Eq. (4) refers to the case of pulse absence: ordinary[5] GMPE depending on geometrical parameters (L and P) is used[6], $G_{Sa|M,L,P}$, and results are weighted for the corresponding pulse absence probability, $P[NoPulse|l,p,e] = 1 - P[Pulse|l,p,e]$. All the other terms are equal to those of Eq. (1), in which pulse-like effects are not considered. Conversely, Eq. (5) refers to the case of pulse occurrence as indicated by the pulse occurrence probability $P[Pulse|l,p,e]$ and by the modified GMPE, $G_{Sa,\text{mod}|T_p,M,L,P}$, in which the additional dependency on T_p, $f_{T_p|M}(t_p|m)$, has to be considered to model the spectral increments around the pulse period according to Eq. (3). Further details on the terms appearing in the equations and not shared by classical PSHA can be found in Chioccarelli and Iervolino (2013).

2.1. NS-PSHA for dip-slip faulting style

Eqs. (4) and (5) can also be written for dip-slip (DS) ruptures. The general framework and numerical procedure are not significantly different from what already shown. In fact, Eq. (2) and all the models introduced in the previous section can be applied; however, minor differences can be identified; they are due to the different geometrical configuration of DS ruptures with respect to SS. More specifically, at least with respect to the issues addressed in this work, DS ruptures cannot be represented by a bi-dimensional scheme (as for the SS case in Fig. 2a), thus (at least) one additional random variable has to be introduced. In Fig. 3 two orthogonal sections of DS rupture are represented assuming the hypothesis of rectangular fault and rectangular rupture.

Eqs. (6) and (7) can be used for DS case considering the following differences with respect to Eqs. (4) and (5):

1) position of the epicentre, E, has to be replaced by the position of the hypocentre (H);
2) the rupture's geometrical parameter dependent on event magnitude is assumed to be the rupture length L, in analogy with the SS case (in principle it should be the area of the rupture from which B and L depend); moreover, the B/L ratio is assumed to be constant for the sake of simplicity;
3) to compute pulse occurrence probability, rupture location within the fault (X_r) is required (for computation of R, along L, P, and H); it is the additional random variable;
4) the introduction of X_r requires knowledge of its PDF conditional to L, $f_{X_r|L}(x_r|l)$:

---

[5] As explained, percentage of pulse-like records in ground motions databases and heterogeneity of pulse periods suggest that directivity effects may be neglected in ordinary GMPEs and the latter can be used for non-pulse hazard contribution. However, a deamplification factor of mean (S_a) predicted by the GMPE of Boore and Atkinson (2008) was recently proposed Shahi and Baker (2011) in the (0 - 10 km) range of R_{jb} (i.e., Joyner and Boore, 1981) distance and for magnitude higher than 6.0. In the same paper, no corrections are suggested for standard deviation of considered GMPE model.

[6] If R_{jb} distance metric is used, GMPE model does not depend on the epicenter's position, E.

$$\lambda_{Sa,NoPulse}(s_a) = v \cdot \int_m \int_l \int_p \int_h \int_{x_r} P[NoPulse|l,p,h,x_r] \cdot G_{Sa|M,X_r,L,P}(s_a|m,l,p,x_r) \cdot$$

$$f_{P,H|L}(p,h|l) \cdot f_{X_r|L}(x_r|l) \cdot f_{L|M}(l|m) \cdot f_M(m) \cdot dm \cdot dl \cdot dp \cdot dh \cdot dx_r \qquad (6)$$

$$\lambda_{Sa,Pulse}(s_a) = v \cdot \int_{t_p} \int_m \int_l \int_p \int_h \int_{x_r} P[Pulse|l,p,h,x_r] \cdot G_{Sa,\mathrm{mod}|T_p,M,X_r,L,P}(s_a|t_p,m,l,p,x_r) \cdot$$

$$f_{T_p|M}(t_p|m) \cdot f_{P,H|L}(p,h|l) \cdot f_{X_r|L}(x_r|l) \cdot f_{L|M}(l|m) \cdot f_M(m) \cdot dt_p \cdot dm \cdot dl \cdot dp \cdot dh \cdot dx_r. \qquad (7)$$

In Chioccarelli and Iervolino (2013) it is shown that numerical results of SS and DS cases have similar general trends independently on the specific rupture mechanism. Thus in the following, SS ruptures are considered for simplicity.
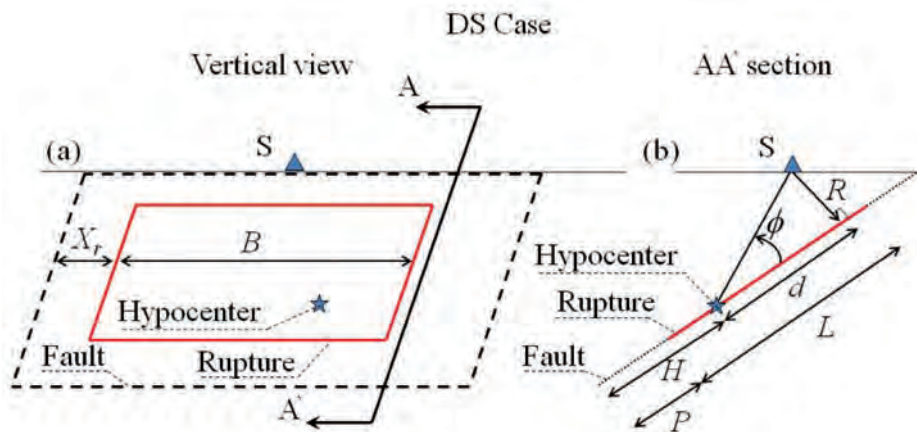

Fig. 3 - DS rupture representations through two vertical and mutually orthogonal sections.

3. Illustrative applications

Preliminary analyses of directivity effects in terms of spectral response were provided by cited studies (i.e., Chioccarelli, 2010; Shahi and Baker, 2011; Chioccarelli and Iervolino, 2013), which address *HIs* due to NS-PSHA with respect to the ordinary one. Results therein show that numerical values of such increments are dependent on geometrical parameters determining the source-to-site configuration, such as fault dimensions and site location. In order to deepen this issue, additional illustrative applications are presented here retaining the hypothesis of known fault geometry, which is common to all the previous works regarding this topic. In fact, the results' sensitivity to uncertainties related to the fault is not discussed here, although believed to be relevant.

As shown in Eqs. (4) and (5), rupture length and rupture position are, in principle, random variables: the former can be assumed lognormal conditional on the event magnitude (Wells and Coppersmith, 1994) and the latter uniformly distributed on the fault. However, applications are

here implemented in the simplifying hypothesis of fixed rupture dimension and position. Such hypothesis appears to be acceptable if a single magnitude can be generated by the considered fault (as assumed in the following). The hypothesis of uniform distribution of the epicenter position on the rupture is retained.

Two cases of single generated magnitude, equal to 5.0 and 6.0, are considered. In Fig. 4a, PDF of T_p (Chioccarelli and Iervolino, 2010) is reported for the two fixed values of magnitude because, as shown in the following section, results are strongly dependent on such distributions.

Starting from the Wells and Coppersmith (1994) prediction model which assumes a lognormal distribution (base 10) of rupture dimension (Fig. 4b), two fixed source length are associated to each magnitude scenario. More specifically, fifth and fiftieth percentiles of rupture length distributions are chosen: 2.0 and 3.4 km SS lengths are associated to M 5.0, while 8 and 14 km are obtained for the M 6.0 scenarios.

In the following, seismic hazard is estimated via the uniform hazard spectrum for a return period (Tr) equal to 475 years; used GMPE is that of Boore and Atkinson (2008); mean annual rate of earthquake occurrence on the fault is 0.05. Attention is focused on HIs if ordinary PSHA is replaced by its modified version for NS sites. In most of the advanced seismic codes worldwide (e.g., CEN, 2003; C.S.LL.PP., 2008), the seismic threat is characterized by UHS computed by ordinary PSHA and quantification of HIs in NS conditions is useful to understand the consequences of neglecting pulse-like directivity effects in hazard analysis. For each spectral period T and for the chosen $Tr = 475$, hazard increments $HI(T)$ are analytically defined by the percentage factor in Eq. (8):

$$HI(T) = \frac{S_a(T)_{NS-PSHA} - S_a(T)_{PSHA}}{S_a(T)_{PSHA}} \cdot 100 \qquad (8)$$

Analyses of a specific site is reported first (Section 3.1), then, contours of $HI(T)$ in the area around the seismic sources are studied for single spectral periods (Section 3.2). This is in order to extend previous site-specific results to a wider area. In fact, contours are also useful
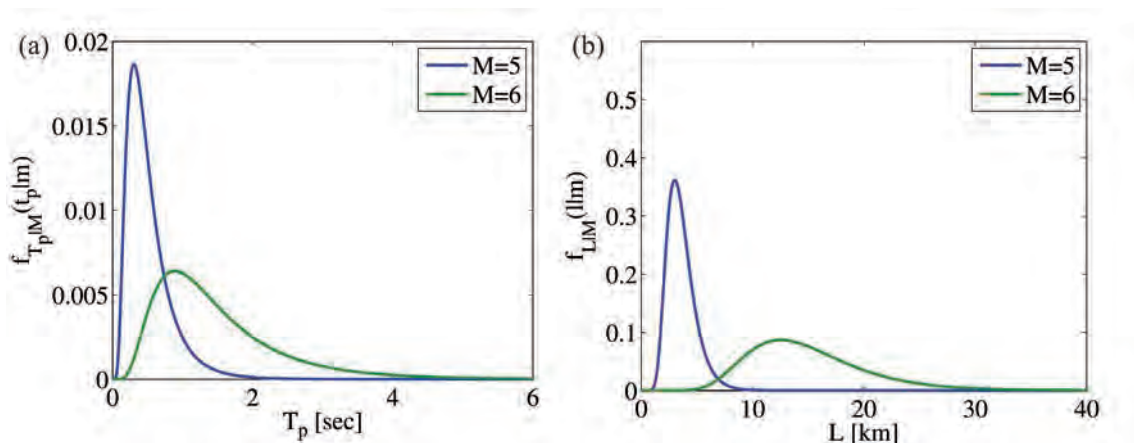

Fig. 4 - Distributions of T_p (a) and L (b) conditional to the used magnitude values.

for identification of the distance from the fault beyond which NS-PSHA provides negligible differences with respect to PSHA.

3.1. Analysis of spectral pulse-like effects for a specific site

A 8 km SS fault is considered with a M 6.0 associated to all generated events (Fig. 5a). UHS are computed with ordinary and modified PSHA for the site in the middle of the fault (site A) where the influence of directivity effects was checked to be the largest (Chioccarelli and Iervolino, 2011; Shahi and Baker, 2011; Chioccarelli and Iervolino, 2013). Pseudo-acceleration response spectra are reported in Fig. 5a while $HI(T)$ are shown in Fig. 5b. As expected, the shape of increments is strictly related to the prediction model of pulse periods (Chioccarelli and Iervolino, 2010) (Fig. 4a) and maximum increments (larger than 100%) affect a range of periods around the median of T_p distribution for M 6.0 (equal to 1.3 s). Conversely, structural periods far from 1.3 s are interested by lower values of $HI(T)$.

Assuming a 2 km SS fault capable of generating M 5 events, UHS and HIs are computed for the site in the middle of the fault (as per the previous case) and are reported in Figs. 6a and 6b, respectively. Again, maximum hazard increments are in accordance with median value of predicted T_p for M 5.0 (Fig. 4a), which is equal to 0.43 s.

It is interesting to note that, in both cases, maximum values of $HI(T)$ are about 100% (107% and 102% for M 5.0 and M 6.0, respectively) which means that NS-PSHA induces actions twice as large than the PSHA in these case-studies. It suggests that, independently on the absolute value of spectral accelerations and on the magnitude of generated events, similar geometrical location of the site on the fault determines similar maximum numerical $HI(T)$. This issue will be verified in Section 3.2.

In both cases, spectral periods interested by maximum $HI(T)$ are closely related to the T_p prediction model (see Fig. 4a), which is dependent on the event magnitude only. This suggests that the fault's characterization, in terms of generated magnitudes, can be used for the prediction of most *dangerous* range of periods which results from NS-PSHA [see Chioccarelli and Iervolino (2010) and Ruiz-Garcìa (2011) for details about the relationship between T_p, T, and inelastic structural demand].
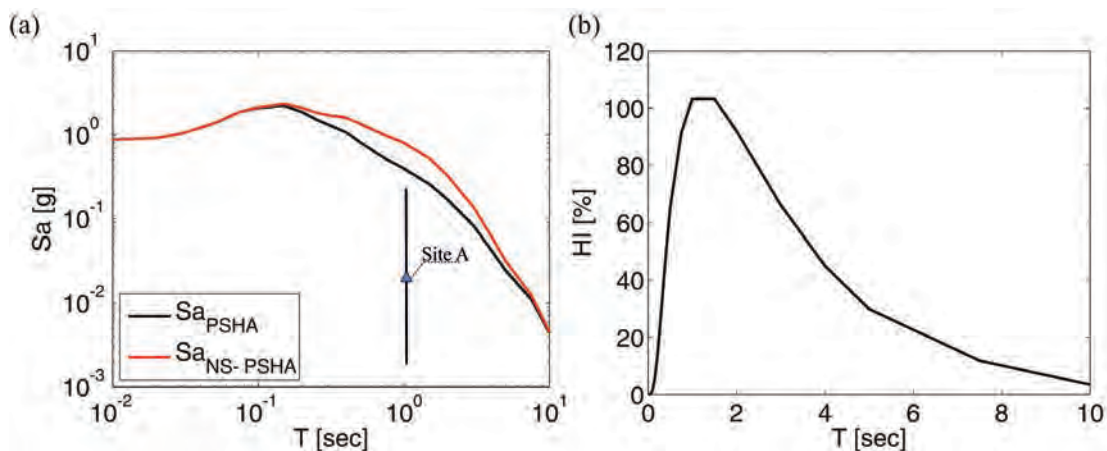

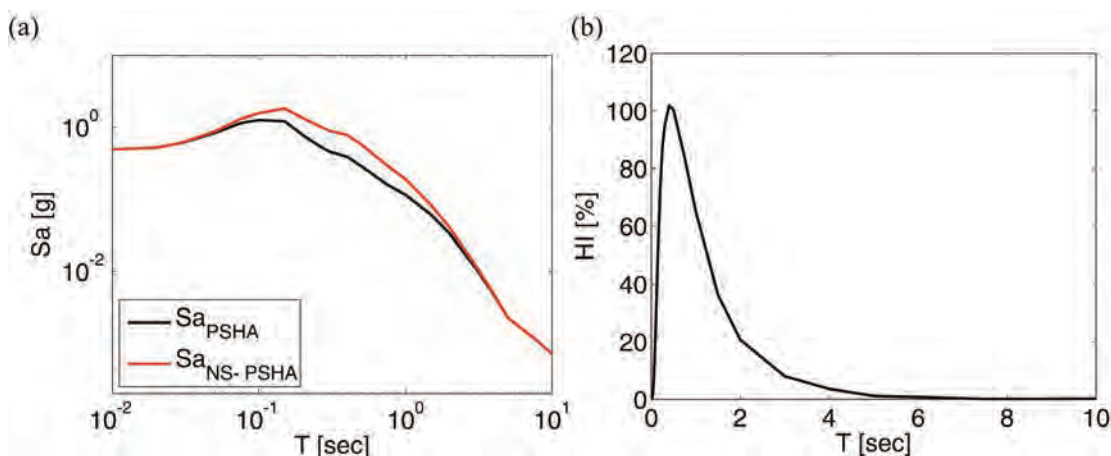Fig. 5 - UHS (a) and *HIs* (b) for site A located in the middle of the 8 km SS fault.

Fig. 6 - UHS (a) and *HIs* (b) for the site located in the middle of the 2 km SS fault.

3.2. Pulse-like-prone near-source areas

In this section the analysis of hazard increments is extended to the whole area affected by the considered sources. UHS and *HIs* were computed for 64 sites influenced by the 8 km SS fault. Studied sites were identified by a 5 by 10 km lattice over a 40 by 60 km area. Results, not shown herein for the sake of brevity, indicate that $HI(T)$ at each site have a similar shape of the site A of Fig. 5b. This is a partly expected result because, in accordance with considered models, and neglecting other possible local effects (which are out of the aim of this work), pulse period distribution (i.e., the shape of $HI(T)$) is dependent only on the event magnitude, which is common to the all sites influenced by the same fault. For this reason, $HI(T)$ are synthetically represented in terms of contours of maximum values at each site (Fig. 7a). Similarly, contours of maximum $HI(T)$ due to a 14 km fault generating *M* 6.0 events are reported in Fig. 7b. In both cases, maximum $HI(T)$ correspond to 1 s spectral period (see Fig. 5).

The case of *M* 5.0 generating fault is also studied with the fault length of 2.0 and 3.4 km (Figs. 7c and 7d, respectively) chosen from Wells and Coppersmith (1994). In these cases, in accordance with Fig. 6b, maximum $HI(T)$ are computed for 0.4 s spectral period.

In all the plots, sites with distances from the rupture higher than 30 km are shaded because a zero pulse probability is associated to them (ordinary and NS-PSHA are formally equivalent).

It should be noted that, for each site in the maps, an approximation of $HI(T)$ in the whole range of spectral period, can be derived applying a scaling factor (*SF*) to $HI(T)$ of Figs. 5b or 6b (depending of the magnitude generated by the fault). Such a *SF* [Eq. (9)] is equal to the ratio between maximum $HI(T)$ reported by contours in the considered site (HI_{site}) and maximum $HI(T)$ of the site in the middle of the fault assumed as reference (HI_{ref}) (i.e., 102% or 107% for *M* 5.0 or 6.0, respectively).

$$SF = \frac{HI_{site}}{HI_{ref}} \qquad\qquad (9)$$

It is also to note that contours of $HI(T)$ are similar even if different generated magnitudes are considered. The reason is the absence of magnitude dependency in the used pulse occurrence
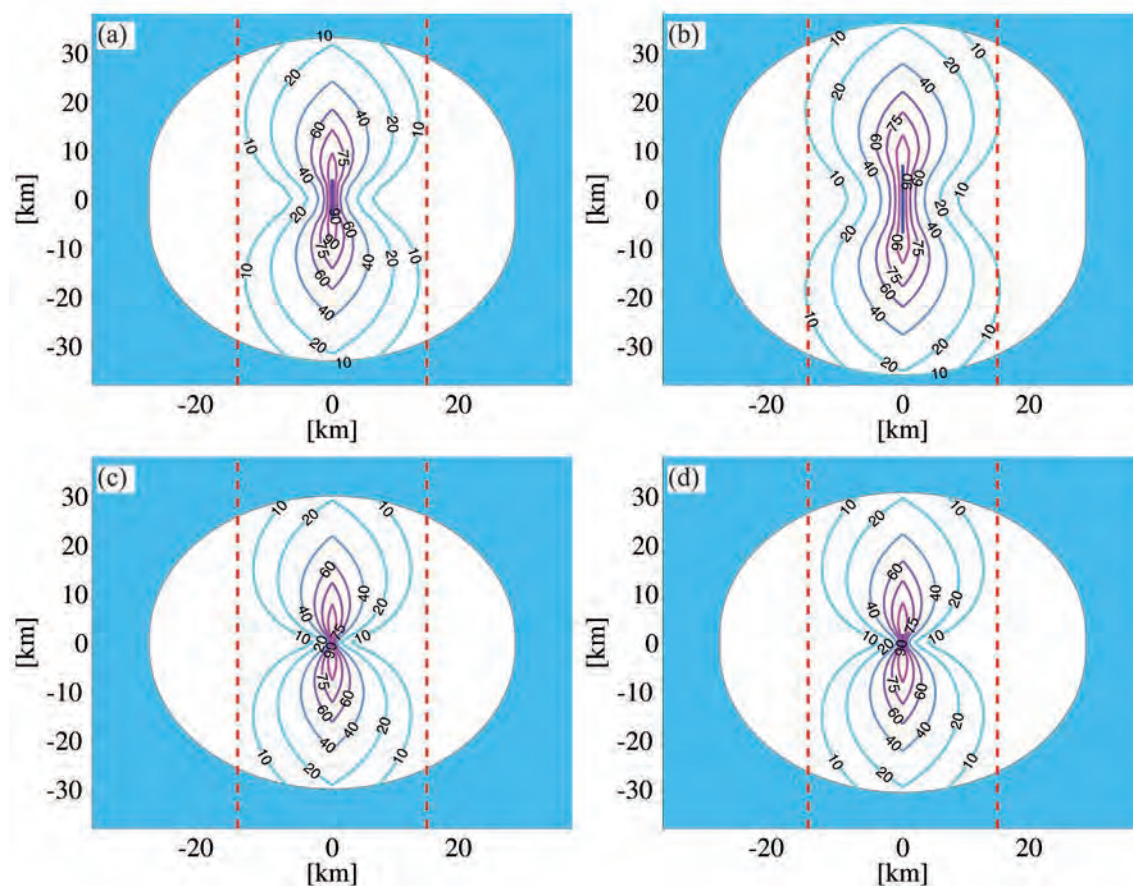
Fig. 7 - Contours of $HI(1s)$ for the 8 (a) and 14 km (b) faults generating M 6.0 events and contours of $HI(0.4s)$ for the 2.0 (c) and 3.4 km (d) faults generating M 5.0 events.

probability model. Two symmetry axes are apparent for the contours, while the elongated shape of $HI(T)$ contours comes from the dependency of pulse occurrence probability on the θ parameter. The minor differences between Figs. 7a, 7b, 7c and 7d depend only on the different rupture lengths. In all cases, the red dotted lines approximate an area near the fault with $HI(T)$ higher than 10%: these lines are 15 km far from the fault and are parallel to it. It means that, at least in these applications, directivity effects can be considered *negligible* for all the sites external to the selected zone (the threshold is arbitrarily chosen).

4. Conclusions

In this work NS-PSHA was briefly recalled along with all the necessary semi-empirical models. Because all of them require the knowledge of size and location of the rupture, illustrative applications are implemented in the case of single fault scenarios. Knowing the seismic sources affecting the construction site is a rational hypothesis for real cases if critical facilities are of concern.

The aim of the illustrative applications was to provide quantitative characterization of

hazard increments due to NS-PSHA with respect to ordinary PSHA. Two specific sites are first considered in the middle of two SS faults generating earthquakes of magnitude equal to 5.0 and 6.0, respectively. In both cases, maximum values of hazard increments are equal to about 100%, that is, NS-PSHA induces elastic actions as large as twice than PSHA.

HIs are found to be strongly dependent on the considered spectral ordinate. Periods to which maximum *HIs* are associated depend on the magnitude of generated events. Thus, more *hazardous* spectral periods can be predicted with the knowledge of the fault's characteristics in terms of generated magnitudes.

Referring to the spectral periods with maximum *HIs* (1.0 or 0.4 s if fault generates *M* 5.0 or *M* 6.0 events, respectively), which are approximated by the median of T_p distribution conditional on magnitude, contours of directivity effects were reported. Because the whole region influenced by the same fault (same magnitude) is expected to be subjected to similar *HI* shapes, contours of maximum *HIs* can be used for deriving an approximation of *HIs* in the whole range of periods for each site multiplying *HIs*, of a reference site, by a site-specific scaling factor.

Shapes of contours are similar even if different generated magnitudes are considered and minor differences could depend only on the different rupture lengths. For investigated cases, it was also possible to geometrically identify the area affected by relevant directivity effects, independently of the specific characteristics of the considered fault in terms of event magnitude. Results suggest that, increasing the number of investigated cases, more general rules can be identified along these same lines.

REFERENCES

Abrahamson N.A.; 2000: *Effects of rupture directivity on probabilistic seismic hazard analysis.* In: Proc. 6th Int. Conf. Seismic Zonation, Palm Springs, CA, 12-15 November 2000, Earthquake Engineering Research Institute.

Baker J.W.; 2008: *Identification of near-fault velocity and prediction of resulting response spectra.* In: Proc. Geotech. Earthquake Eng. Struct. Dyn. IV, Sacramento, CA, USA, 10 pp.

Boatwright J. and Boore D.M.; 1982: *Analysis of the ground acceleration radiated by the 1980 Livermore valley earthquake for directivity and dynamic source characteristics.* Bull. Seismol. Soc. Am., **72**, 1843-1865.

Boore D.M. and Atkinson G.M.; 2008: *Ground-motion prediction equations for the average horizontal component of PGA, PGV and 5% damped PSA at spectral period between 0.01 s and 10.0 s.* Earthquake Spectra, **24**, 99-138.

CEN; 2003: *Eurocode 8: Design Provisions for Earthquake Resistance of Structures, Part 1.1: general rules, seismic actions and rules for buildings, PrEN1998-1.* European Committee for Standardization TC250/SC8/, Brussels, Belgium.

Chioccarelli E.; 2010: *Design earthquakes for PBEE in far-field and near-source conditions.* **PhD Thesis,** Dipartimento di Ingegneria Strutturale, Università degli Studi di Napoli Federico II, Napoli, Italy, http://www.dist.unina.it/doc/tesidott/PhD2010.Chioccarelli.pdf.

Chioccarelli E. and Iervolino I.; 2010: *Near-source seismic demand and pulse-like records: a discussion for L'Aquila earthquake.* Earthquake Eng. Struct. Dyn., **39**, 1039-1062.

Chioccarelli E. and Iervolino I.; 2011: *Near-source design scenarios for critical facilities.* **In: Proc. 30° Convegno** Gruppo Nazionale di Geofisica della Terra Solida (GNGTS), Trieste, Italy, pp. 243-245.

Chioccarelli E. and Iervolino I.; 2013: *Near-source hazard and design scenarios*. Earthquake Eng. Struct. Dyn., **42**, 603-622.

Cornell C.A.; 1968: *Engineering seismic risk analysis*. Bull. Seismol. Soc. Am., **58**, 1583-1606.

C.S.LL.PP.; 2008: *DM 14 gennaio 2008, Norme Tecniche per le Costruzioni*. Gazzetta Ufficiale della Repubblica Italiana, 29, Roma, Italy, in Italian.

Iervolino I. and Cornell C.A.; 2008: *Probability of occurrence of velocity pulses in near-source ground motions*. Bull. Seismol. Soc. Am., **98**, 2262-2277.

Iervolino I., Chioccarelli E. and Baltzopoulos G.; 2012: *Inelastic displacement ratio of near-source pulse-like ground motions*. Earthquake Eng. Struct. Dyn., **41**, 2351-2357, doi:10.1002/eqe.2167.

Joyner W.B. and Boore D.M.; 1981: *Peak horizontal acceleration and velocity from strong-motion records including records from the 1979 Imperial valley, California earthquake*. Bull. Seismol. Soc. Am., **71**, 2011-2038.

McGuire R.K.; 2004: *Seismic hazard and risk analysis*. Earthquake Eng. Res. Inst., Oakland, CA, USA, Report MNO-10, 240 pp.

Meletti C., Galadini F., Valensise G., Stucchi M., Basili R., Barba S., Vannucci G. and Boschi E.; 2008: *A seismic source zone model for the seismic hazard assessment of the Italian territory*. Tectonophys., **450**, 85-108.

Ruiz-Garcìa J.; 2011: *Inelastic displacement ratios for seismic assessment of structures subjected to forward-directivity near-fault ground motions*. J. Earthquake Eng., **15**, 449-468.

Shahi S. and Baker J.W.; 2011: *An empirically calibrated framework for including the effects of near-fault directivity in probabilistic seismic hazard analysis*. Bull. Seismol. Soc. Am., **101**, 742-755.

Somerville P.G., Smith N.F., Graves R.W. and Abrahamson N.A.; 1997: *Modification of empirical strong motion attenuation relations to include the amplitude and duration effect of rupture directivity*. Seismol. Res. Lett., **68**, 199-222.

Spudich P. and Chiou B.S.J.; 2008: *Directivity in NGA earthquake ground motion: analysis using isochrones theory*. Earthquake Spectra, **24**, 279-298.

Tang Y. and Zhang J.; 2010: *Response spectrum-oriented pulse identification and magnitude scaling of forward directivity pulses in near-fault ground motions*. Soil Dyn. Earthquake Eng., **31**, 59-76, doi:10.1016/j.soildyn.2010.08.006.

Tothong P., Cornell C.A. and Baker J.W.; 2007: *Explicit directivity-pulse inclusion in probabilistic seismic hazard analysis*. Earthquake Spectra, **23**, 867-891.

Wells D.L. and Coppersmith K.J.; 1994: *New empirical relationships among magnitude, rupture length, rupture width, rupture area, and surface displacement*. Bull. Seismol. Soc. Am., **87**, 974-1002.

Corresponding author: Eugenio Chioccarelli
                            Dipartimento di Ingegneria Strutturale,
                            Università degli Studi di Napoli, via Claudio 21, 80125 Naples, Italy
                            Phone: +39 081 7683669; fax: +39 081 7685129; e-mail: eugenio.chioccarelli@unina.it